Low-Noise Ku-band Receiver Frontend with Switchable SIW filters for Cubesat Applications

G. Orecchini [1], G. Schiavolini [1], P. Mezzanotte [1], F. Dogo [2,3], S. Pauletto [2], A. Beltramello [2], D. Manià [2], V. Palazzi [1], G. Simoncini [1], L. Roselli [1], A. Gregorio [2,3], M. Fragiacomo [2], F. Alimenti [1]

[1]*Department of Engineering, University of Perugia, via G. Duranti 93, I-06125 Perugia, Italy*
[2]*PICOSATS s.r.l., Area Science Park, Padriciano 99, 34127 Trieste, Italy*
[3]*Department of Physics, University of Trieste, via Valerio 2, 34149 Trieste, Italy*
federico.alimenti@unipg.it

***Abstract*—This paper proposes a low-noise receiver frontend for nanosatellite and Cubesat platforms. The frontend is composed by a Low-Noise Amplifier (LNA) and two Substrate Integrated Waveguide (SIW) filters, providing a frequency reconfigurability to the system. The two filters operate in the 13 and in the 14 GHz uplink bands, and are selected by means of a pair of solid-state SPDT switches. As a results, 15.5 dB gain with 2.4 dB noise figure for the 13 GHz configuration and 17.8 dB gain with 2.3 dB noise figure for the 14 GHz configuration are obtained. This work is important since demonstrates a low-cost solution for satellite radio apparatuses based on commercial components on a standard PCB.**

***Index Terms*—Nanosatellites, CubeSats, RF/microwave electronics, Ku-band transponders.**

I. Introduction

Nanosatellites and Cubesats are miniaturized platforms with enormous potential for science, telecommunication and, more in general, for future space-based services like the Internet of Space (IoS), [5]- [5], [1]. In the IoS scenario, Cubesats not only plays the role of network infrastructure bringing the Internet to remote places, but they will provide connecting capabilities to sensors that, in principle, can be located everywhere in the world, [7], [8].

As a consequence of the space market expansion, high performance radio transceivers and transponders are becoming increasingly important in commercial and scientific missions to guarantee the above connectivity. According to the Cubesats design approach, these radios should be low-cost and based con Components Off The Shelf (COTS), i.e. based on Si or GaAs integrated circuits already developed for automotive or military telecommunication purposes, [2], [3].

The State-of-the-Art (SoA) for satellite radio receivers includes: fully integrated frontends [11], apparatuses based on COTS [13], and systems exploiting hybrid modules [12]. The latter modules are realized by wire bonding naked GaAs chips to a distributed microwave circuit fabricated on a low-loss substrate (in this sense they are "hybrid"). Then they are connected together to implement all the receiver functions, and placed into a metal housing with cavities shielding the different receiver stages. The result is very reliable but bulky.

Frequency reconfigurability is another important issue. This has already been addressed by some authors by means of tunable filters. Varactors or Micro Electro-Mechanical Systems (MEMS) have been used to this purpose, [9], [10].

In the present contribution we present, for the firs time, a Ku-band frontend that features a frequency reconfigurability in two sub-bands, namely the 13-GHz and the 14-GHz uplink sub-bands allocated for GEO satellite services. The developed circuit is completely based on COTS and use two Substrate Integrated Waveguide (SIW) filters that can be connected to a single input Low-Noise Amplifier (LNA) by means of solid-state switches. The SIW filters are self-shielded devices. In this way the receiver can be completely integrated into a commercial Printed Circuit Board (PCB), and complex mechanical designs with shielding cavities are avoided. This design approach is experimentally validated in the present contribution, opening the way to a novel generation of low-cost, reconfigurable satellite radios.

II. System overview

The considered system is a transponder operating in the Ku-band allocated for the GEO stationary space services. An uplink signal between 12.50 to 14.80 GHz (coming from a ground station) is received, amplified, filtered, frequency converted and transmitted back to Earth in a different direction. The downlink frequency range is between 10.70 to 12.75 GHz. The simplified block diagram of the transponder is shown in Fig. 1. No demodulation, error correction and modulation functions are present in the apparatus so that the transponder is "transparent" to the modulation scheme adopted. With this approach any signal and waveform can be managed by the radio, provided that it falls within the $0.5\,\mathrm{MHz}$ system bandwidth. The uplink signals are received by the transponder and will be also denoted as RX signals; the downlink signals are transmitted and will be also denoted as TX signals.

The system operates in full-duplex mode, simultaneously transmitting a receiving signals with the same horn antenna. These two paths use orthogonal linear polarizations: vertical (V) for the transmitter, and horizontal (H) for the receiver. An Ortho-Mode Transducer (OMT) separates TX and RX signals, providing an isolation of about 70 dB between these ports. A self interference, however, is generated in the system because of finite OMT isolation. Since a 10 W (or 40 dBm) transmitter

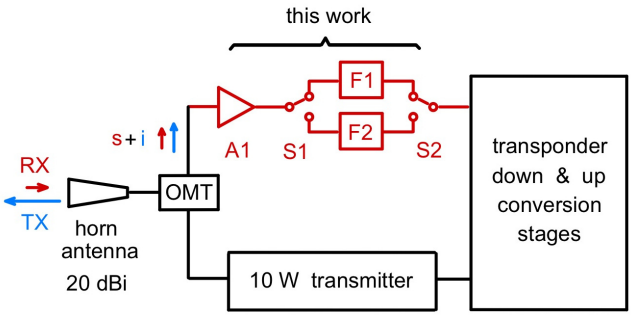

Fig. 1. Simplified block diagram of the Ku-band transponder. The system operates in full-duplex mode, simultaneously transmitting and receiving signals with a single horn antenna in orthogonal polarization. An Ortho-Mode Transducer (OMT) separates TX and RX signals, but a self interference ("i" in the figure) is generated. The self interference level is much greater than the received signal ("s" in the figure) level. To increase immunity a switchable filter configuration is adopted in the receiver frontend. A1: 27 dB LNA; F1: 13 GHz filter; F2: 14 GHz filter; S1 and S2 solid-state switches.

is adopted, the self interference power level ("i" in the figure) is estimated to be around -30 dBm and is much greater than the received signal level ("s" in the figure), that is in the order of -100 dBm. Since uplink and downlink frequency bands overlap, a single image-reject filter cannot be use in the the receiver. To increase the immunity to self interference, a switchable filter configuration (F1 and F2 in the figure) is adopted in the receiver frontend. The low-cost implementation of such a configuration is the originality element of the present contribution. The receiver frontend is composed by a Low-Noise Amplifier or LNA (A1), a first 13-GHz SIW bandpass filter (F1), a second 14-GHz SIW bandpass filter (F2), and two SPDT switches (S1 and S2) needed to configure the system.

The main system requirements for the transponder receiver are reported in Tab. I. They are referred to a GEO stationary orbit at 36000 km, and have been obtained with a detailed link-budget analysis. G^a_{tx} is the ground station antenna gain (uplink), resulting in a 103 dBm EIRP for a 50 W transmitter. G^a_{rx} and P_{rx} are the receiver antenna gain and input power level. The path loss is referred to clear sky conditions, but the system should tolerate up to 5 dB of atmospheric losses.

TABLE I
KU-BAND GEO LINK BUDGET AND RECEIVER REQUIREMENTS

f_0 (GHz)	G^a_{tx} (dBi)	EIRP (dBm)	path loss (dB)	G^a_{rx} (dBi)	P_{rx} (dBm)
12.5-14.8	56.0	103	216	15	-98

III. MATERIALS AND METHODS

In order to keep low the transponder production costs, a commercial PCB technology is adopted. The PCB stackup is composed by 4-layers, with the top and bottom ones made out of RO4350B material (thickness 254 μm, $\epsilon_r = 3.48$, $\tan\delta = 0.004$), and the two internal ones implemented with FR4 material (thickness 508 μm including prepreg, $\epsilon_r = 4.6$, $\tan\delta = 0.02$). With the chosen fabrication process it is possible to realize a minimum track width and a spacing of 0.15 mm, a minimum via diameter of 0.2 mm, and to fabricate buried via interconnections.

The LNA (A1 in Fig. 1) and the two solid-state SPDT switches (S1 and S2 in Fig. 1) are COTS already available on the electronic market. The LNA shows a 27 dB power gain, a 1.4 dB noise figure and a current consumption of 54 mA at 3 V. The amplifier linearity (-15 dBm input 1 dB compression point and -3 dBm input third-order intercept point) is enough to tolerate the -30 dBm self interference without saturation or significant desensitation. The two solid-state, non-reflective GaAs switches have an insertion loss of 2.2 dB, an isolation of 40 dB and a current consumption of 10 μA at -5 V supply.

As previously illustrated, a front-end with switchable image-reject filter is adopted because TX (downlink) and RX (uplink) bands overlap. Although not shown in Fig. 1 the first Intermediate Frequency (IF) of the receiver is set to 2185 MHz. The uplink frequency range is so divided into two sub-bands, namely: the 13-GHz sub-band from 12.75 to 13.25 GHz and the 14-GHz sub-band from 13.75 to 14.8 GHz. The 500 MHz transition band from 13.25 to 13.75 GHz cannot be used, but this is acceptable for the considered application.

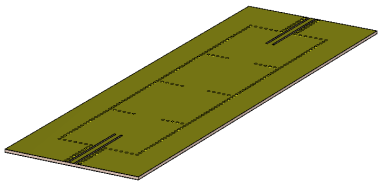

Fig. 2. 13 GHz SIW filter layout used in the electromagnetic simulations. Note the GCPW to SIW input and output transitions implementing the impedance transformations required by the filter.

The filters are implemented in SIW technology according to [14], because the devices are self shielded and fully integrated in the PCB (i.e. no external components are needed). These devices are constituted by four resonant cavities coupled with inductive irises, and include input/output Grounded Co-Planar Waveguide (GCPW) to SIW transitions, working also as impedance transformers (the filters require precise termination impedances). The design method is based on the approach suggested, in 2008, by Wu *et al.*, [15]. Such a methodology makes extensive usage of 3D electromagnetic simulations: the final 13-GHz filter layout is reported in Fig. 2.

IV. RESULTS

The proposed concept is validated in two steps. First a SIW filter breadboard is fabricated and characterized with the Vector Network Analyzer (VNA). A 10 MHz to 40 GHz Agilent N5230A, equipped with an automatic (full two port) calibrator, is used to this purpose. Fig. 3 illustrates the fabricated prototypes (top panel) and the comparison between measured and simulated scattering parameters (bottom panels).

The two filters are correctly tuned to the specified frequency bands. Simulations and measurements are in good agreement, apart for an underestimation of the insertion losses. These

are due to tolerances in the substrate material dissipation factor, and to the coaxial to microstrip adapters, that were not considered in the electromagnetic model. The center frequency insertion losses are: 6.8 dB measured against 3.4 dB simulated (for the 13 GHz filter); 4.4 dB measured against 2.0 dB simulated (for the 14 GHz filter).

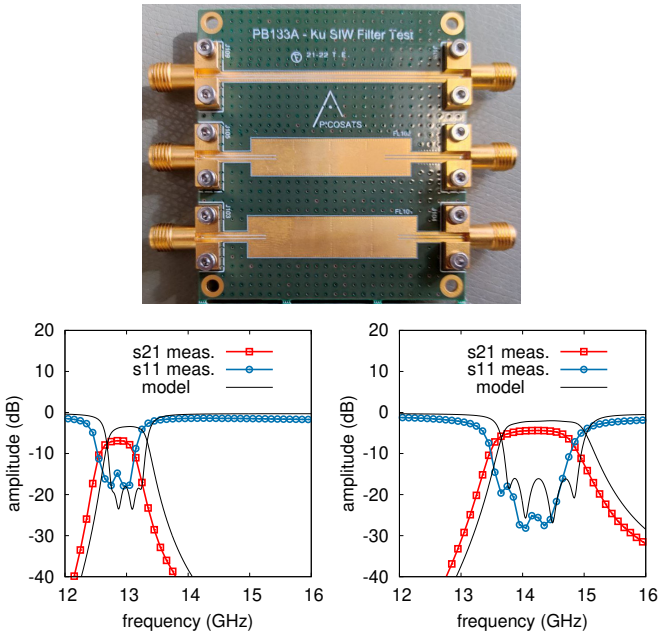

Fig. 3. Fabricated test PCB with SIW filters and calibration line (top) and comparison between measured and simulated scattering parameters (bottom). 13 GHz filter response (bottom left); 14 GHz filter response (bottom right). Simulations agrees well with measurements apart for an underestimation of the insertion losses, due to both substrate material and coaxial adapters. Center frequency insertion losses: 6.8 dB measured against 3.4 dB simulated (13 GHz filter); 4.4 dB measured against 2.0 dB simulated (14 GHz filter).

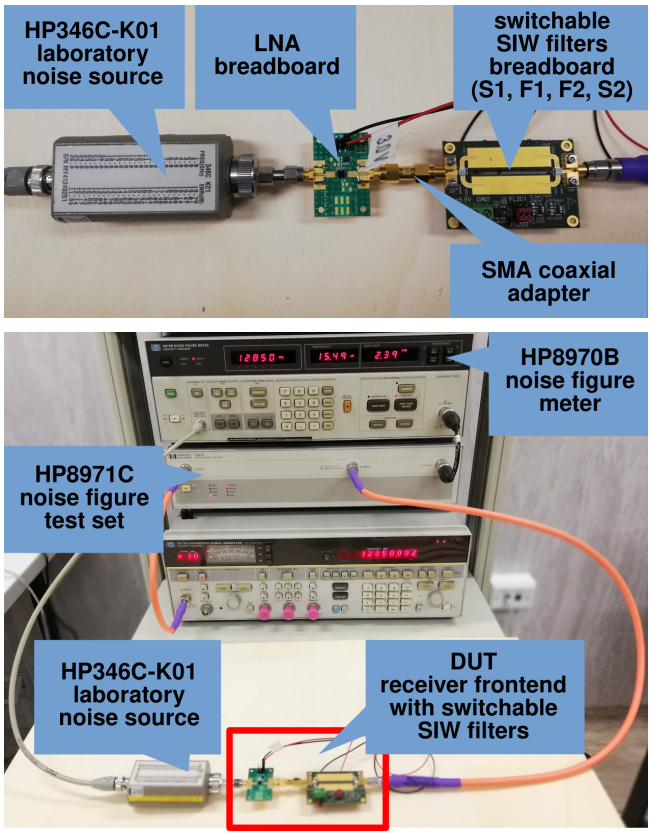

Fig. 4. Receiver frontend breadboard (top) and experimental setup (bottom). An HP8970S noise figure test set is used for the experimental characterization of the breadboard. The test set is calibrated by means of a HP346c-K01 laboratory noise source. Data are acquired automatically with a Python script. As a further verification the frontend scattering parameters are measured with a VNA (experimental not shown here).

As a second step, the two SIW filters are combined with the solid-state switches S1 and S2, and another test PCB is fabricated. An on-board DC-DC converter is used to generate the negative voltage supply needed by the switches (equal to -5 V). The receiver frontend breadboard is finally implemented as in Fig. 4 (top panel), by cascading LNA and switchable filter PCBs. These two circuits are connected with a SMA coaxial adapter. An HP8970S noise figure test set is used for the experimental characterization of the frontend (see Fig. 4, bottom panel). The test set is calibrated by means of a HP346c-K01 (1 to 50 GHz) laboratory noise source. Data are acquired automatically with a Python script. As a further verification the frontend scattering parameters are measured with the VNA.

Fig 5 shows the measured power gain and noise figure of the whole receiver frontend. The two groups of curves are obtained by simply switching S1 and S2 in the 13 and 14 GHz switch configurations. The center frequency performance (coaxial adapetr including) are: 15.5 dB gain and 2.4 dB noise figure (for the 13 GHz configuration); 17.8 dB gain and 2.3 dB noise figure (for the 14 GHz configuration). The frontend draws a current of about 54 mA at 3 V, mostly due to the LNA; the current related to the switches and to their DC-DC converter is practically negligible. The overall power consumption is about 162 mW.

Large signal frontend measurements gives input-referred 1 dB compression point and third-order intercept point in good agreement with those reported, by the manufacturer, for the LNA alone. The obtained results demonstrate the feasibility of a low-noise receiver frontend operating in the Ku-band and completely based on COTS components.

Finally a comparison of the previous results with the present State-of-the-Art for Ku-band satellite receivers is reported in Tab. II. The work of Roy et *al.* [12] shows an apparatus that is very close to ours for both mission scenario (GEO satellites) and sensitivity. Such a receiver, however, uses hybrid circuits, is bulky and cannot be reconfigured in frequency (operates only in our lower sub-band). The work of Malmqvist et *al.* [9], instead, proposed a tunable monolithic solution based on MEMS varactors. This circuit feature an impressive miniaturization, but needs a custom microelectronic facility to be fabricated and, at the moment, is not available on the market as a COTS.

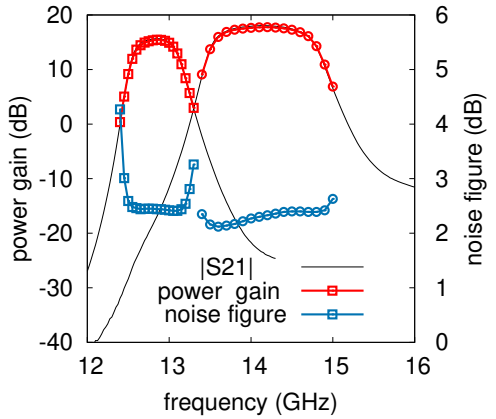

Fig. 5. Measured power gain and noise figure of the whole receiver frontend for the 13 and 14 GHz switch configurations. Center frequency performance (coaxial adapetr including): 15.5 dB gain and 2.4 dB noise figure (13 GHz configuration); 17.8 dB gain and 2.3 dB noise figure (14 GHz configuration). The frontend draws a current of about 54 mA at 3 V (LNA) and of 7 mA at 5 V (both switches). The overall power consumption is less than 162 mW.

TABLE II
KU-BAND RECEIVERS STATE-OF-THE-ART

Ref.	Mission Scenario	f_0 (GHz)	Gain (dB)	F_{RX} (dB)	DC (W)	Mass (kg)
[12]	GEO telecommand and ranging	12.8-13.3	9 (+)	3.2	10 (-)	n.a.
[9]	UAV and aeronautics	8.0-10.0	15	2.9	0.15	(*)
this work	GEO bring into use	12.5-14.8	15-17	2.5	0.16	0.1

(+) frontend only; (-) whole receiver; (*) monolithic solution

V. CONCLUSIONS

This work demonstrates that Ku-band satellite radio receivers based on commercial technologies are feasible at low-cost. A configuration with LNA and switchable SIW filters is demonstrated for the first time. 15.5 dB gain with 2.4 dB noise figure for the 13 GHz configuration and 17.8 dB gain with 2.3 dB noise figure for the 14 GHz configuration are obtained. The achieved electrical performance compares well with the present State-of-the-Art: the receiver circuit is sufficiently miniaturized to stay in a Cubesat, can be fabricated with commercial PCB technology and doesn't require complex shielding mechanics.

ACKNOWLEDGEMENTS

This work was supported in part by the the Italian Ministry of University and Research (MUR), in the frame of the "PON 2022 Ricerca e Innovazione" action.

REFERENCES

[1] A. Gregorio and F. Alimenti, "Cubesats for future science and internet of space: Challenges and opportunities," in *IEEE International Conference on Electronics, Circuits and Systems (ICECS)*, Bordeaux (F), Dec. 2018.

[2] F. Alimenti and et al., "K/Ka-band very high data-rate receivers: A viable solution for future Moon exploration missions," *MDPI Electronics*, vol. 8, no. 3, pp. 1–23, Mar. 2019.

[3] F. Alimenti, P. Mezzanotte, G. Simoncini, V. Palazzi, R. Salvati, G. Cicioni, L. Roselli, F. Dogo, S. Pauletto, M. Fragiacomo, and A. Gregorio, "A ka-band receiver front-end with noise injection calibration circuit for cubesats inter-satellite links," *IEEE Access*, vol. 8, pp. 106 785–106 798, Jun. 2020.

[4] F. Berrilli, A. Bigazzi, L. Roselli, P. Sabatini, M. Velli, F. Alimenti, F. Cavallini, V. Greco, P. Moretti, S. Orsini, M. Romoli, S. White, and the ADAHELI Team, "The ADAHELI solar mission: Investigating the structure of the sun's lower atmosphere," *Advances in Space Research*, vol. 45, no. 10, p. 1191–1202, May 2010.

[5] *Achieving Science with CubeSats: Thinking Inside the Box*, The National Academies Press, Washington, DC, USA, 2016. [Online]. Available: https://www.nap.edu/catalog/23503/achieving-science-with-cubesats-thinking-inside-the-box

[6] N. Chahat, "A mighty antenna from a tiny cubesat grows," *IEEE Spectrum*, vol. 55, no. 2, pp. 32–37, Feb. 2018.

[7] M. Mitry, "Routers in space: Kepler communications' CubeSats will create an Internet for other satellites," *IEEE Spectrum*, vol. 57, no. 2, pp. 38–43, Feb. 2020.

[8] M. Harris, "Tech giants race to build orbital internet," *IEEE Spectrum*, vol. 55, no. 6, pp. 10–11, Jun. 2018.

[9] R. Malmqvist, A. Ouacha, and R. Erickson, "Multi-band and reconfigurable front-ends for flexible and multi-functional rf systems," in *Asia-Pacific Microwave Conference*, Bangkok, Thailand, Dec. 2007, pp. 1–4.

[10] M. Schuhler, A. Jaschke, and A. Popugaev, "Reconfigurable rf receiver front-end for cognitive radio," in *Microelectronic Systems*, A. Heuberger, G. Elst, and R. Hanke, Eds. Berlin, Heidelberg: Springer, 2011.

[11] S. Hsu, P.-Y. Wang, P.-C. Su, M.-C. Chou, Y.-C. Chang, and D.-C. Chang, "Design of ku/ka band down-converter front-end for digital broadcast satellite receivers," in *IEEE International Wireless Symposium (IWS)*, Shenzhen, China, Mar. 2015, pp. 1–4.

[12] D. Roy, A. Choudhury, M. Mohiyuddin, A. Sucharitha, and D. Ramana, "Design and realisation of ku-band tele-command and ranging receiver for satellite application," in *IEEE MTT-S International Microwave and RF Conference (IMaRC)*, Kolkata, India, Nov. 2018, pp. 1–4.

[13] G. D. Andrade, E. Barbosa, and S. Rondineau, "Rf front-end receiver for vehicular satellite communications and lna gaas fet design in ku-band," in *Workshop on Communication Networks and Power Systems (WCNPS)*, Brasilia, Brazil, Nov. 2020, pp. 1–6.

[14] F. Alimenti, P. Mezzanotte, V. Palazzi, L. Roselli, F. Dogo, and M. Fragiacomo, "Microwave receiver device," European Patent 21 169 960.8, Apr. 21, 2021.

[15] X.-P. Chen and K. Wu, "Substrate integrated waveguide cross-coupled filter with negative coupling structure," *IEEE Trans. on Microwave Theory and Techniques*, vol. 56, no. 1, pp. 142–149, Jan. 2008.